Paper CIT06-0526

DESIGN OPTIMIZATION OF AXIAL-FLOW HYDRAULIC TURBINES USING GEOMETRICAL PARAMETERIZATION AND THE RADIAL EQUILIBRIUM EQUATION

Rodrigo Barbosa da Fonseca e Albuquerque
Federal University of Itajubá – UNIFEI; Av. BPS, 1303, C. P. 50, CEP 37500-903, Itajubá, MG, Brazil.
galegosigma@yahoo.com.br

Nelson Manzanares Filho
Federal University of Itajubá – UNIFEI; Av. BPS, 1303, C. P. 50, CEP 37500-903, Itajubá, MG, Brazil.
nelson@unifei.edu.br

Waldir de Oliveira
Federal University of Itajubá – UNIFEI; Av. BPS, 1303, C. P. 50, CEP 37500-903, Itajubá, MG, Brazil.
waldir@unifei.edu.br

Abstract. This paper presents the development of a low cost computational methodology for the conceptual design optimization of axial-flow hydraulic turbines (propeller turbines). The methodology has been developed with a quasi-two dimensional flow model, employing empirical correlations for cascade losses and flow deviations. As in a previous work, the study is based on the conservation principles for mass and angular momentum, but now it is included the radial equilibrium equation in order to achieve a more realistic flow field. For reducing the number of design variables, the runner blading stagger, chord-pitch ratio and camber are parameterized in terms of their values at the hub, mean and tip stations. The design optimization algorithm has been coded in MATLAB™ language. This code searches for a basic geometry that maximizes the turbine efficiency, given the design flow rate, rotational speed and bounds for the design variables and also for the available head. Two optimization techniques have been applied: a standard sequential quadratic programming, which searches for local maximizers starting from an initial point, and a controlled random search algorithm, a population set-based algorithm that searches for global maximizers starting from an initial population. An application example of the methodology is presented and discussed for the optimization of a real turbine model, previously tested in a laboratory rig. The optimized solution is compared with original turbine design, showing the performance improvements, according to the hydrodynamic modeling. Recommendations for methodology improvements are also made.

Keywords. axial-flow hydraulic turbine, loss and deviation modeling, geometry parameterization, optimization technique, design optimization.

1. Introduction

Hydraulic turbines have been designed for about two hundred of years. In the early designs, the engineer own experience and trial-and-error tests with models represented the main available design tools. The amount of empirical information was comparable with the feasible analytical methods based on theory. A fraction of this empirical knowledge was condensed in several design charts – used even today – which furnish guidelines for some turbine basic dimensions (Cordier, 1955; Schweiger and Gregori, 1989). Another portion of this knowledge has been retained by the engineers themselves, being transmitted, as an inheritance, to next engineer teams of the companies.

The development of computers in the second half of twenty century made possible the use of complex numerical flow simulation methods for turbine analysis and design. Nowadays, 3D Euler codes and 3D viscous Navier-Stokes codes are already standard tools on the development of new water turbine units. Details of flow separation, loss sources, loss distribution in components, matching of components at design and off-design, and low pressure levels with risk of cavitation are now amenable to analysis with computational fluid dynamics – CFD (Drtina and Sallaberger, 1999).

The application of these modern CFD techniques for predicting the flow through an entire turbine has brought further substantial improvements in its hydraulic design. Since the detailed understanding of flow phenomena is of great practical importance, it has a direct impact on the design, resulting in geometrical changes of existing components, the replacement of existing components by a completely new design and/or the use of new materials (Drtina and Sallaberger, 1999).

Although 3D Navier-Stokes codes have shown most reliable results, with accurate performance predictions and flow details, hence decreasing the number and costs of model tests, a significant amount of computational effort has to be spent with grid generation and grid modification in each numerical investigation. For instance, in turbomachine design optimization, the context of the present work, when a geometrical modification is made by the optimization algorithm, the meshes must be recalculated and the flow solver – with its high computational cost – must be run again. This effort often prevents the integration of sophisticated Navier-Stokes simulations into the whole design procedure. In addition, a fast, simple and reasonable accurate analysis is still essential for the initial design phases, when the geometry is not yet all determined (Oh and Kim, 2001; Yoon *et al.*, 1998).

Therefore it would be desirable to make available intermediate design optimization schemes – with low computational cost – for turbomachines. These schemes must furnish a reliable conceptual design, with a simplified but representative geometry for runners and stators and also the correct trends towards the optimum flow field. In the present work, such a methodology is proposed for axial-flow hydraulic turbines. From its results, then, one could use a more sophisticated CFD code to make the refinements only (Lipej, 2004; Peng *et al.*, 2002), what would substantially decrease total computation time.

2. Formulation of the optimization problem

In this section, we describe the turbine design optimization problem. In guidelines, it consists on searching some runner blade and guide vane basic geometries (design variables) in order to maximize the turbine efficiency (objective function), given the design rotational speed and volumetric flow rate (design point optimization only). The available head may lay within upper and lower bounds, these being the nonlinear constraints of the problem. There are also lateral constraints for the design variables, defining problem feasible region.

Formally, this can be stated as a constrained minimization problem as follows:

minimize $f(\mathbf{x})$
subject to $g_i(\mathbf{x}) \leq 0$, $i = 1, ..., m$.
$\mathbf{x} \in S$

$\mathbf{x}$ is the n-dimensional vector of design variables (x_j, $j = 1, ..., n$). The feasible region S is defined by upper and lower bounds, x_j^U and x_j^L respectively, for each coordinate of $\mathbf{x}$: $S = \{\mathbf{x} \in \Re^n : x_j^L \leq x_j \leq x_j^U , j = 1, ..., n\}$. The objective function is $f(\mathbf{x}) = -\eta(\mathbf{x})$, where η is the turbine efficiency (single objective optimization). $g_i(\mathbf{x})$, $i = 1, ..., m$, are the m constraint functions, namely, $g_1(\mathbf{x}) = H_L - H(\mathbf{x})$ and $g_2(\mathbf{x}) = H(\mathbf{x}) - H_U$, where H is the turbine available head and H_L and H_U are respectively lower and upper bounds, such that $H_L \leq H \leq H_U$.

Another way to impose the available head constraints is by means of a penalization scheme on objective function:

$$f = \begin{cases} -\eta + M(H_L - H)^2, & H < H_L \\ -\eta, & H_L \leq H \leq H_U \\ -\eta + M(H - H_U)^2, & H > H_U \end{cases}$$

Here, M is a "big" positive number. Again, the objective is to maximize η (minimize $-\eta$) with H laying in the interval $[H_L ; H_U]$. The choice of the penalty factor M must not drive the optimization process towards a penalty minimization only, missing objective function main information, i.e., the efficiency η. Also, the constraints must not be violated at the end of the process. Some tests have to be performed to settle suitable values for M.

Although the evaluation of cavitation performance is a basic feature in hydraulic turbine design, the present work is concerned only with the turbine efficiency. Actually, the cavitation occurrence may be preliminarily avoided by controlling the blade incidence angles and loading distributions. By specifying some criteria like these, one may run the turbine efficiency optimization code with some safety against cavitation risk. Thereafter a more sophisticated blade design CFD technique can be used to refine the previous solution, ensuring minimum cavitation occurrence (Lipej, 2004; Peng *et al.*, 2002).

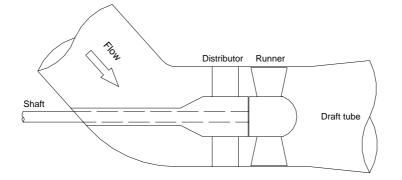## 3. Flow calculation through an axial-flow hydraulic turbine

3.1. General

The water turbine considered in this study is a tube type propeller turbine with non-adjustable guide vanes, as Fig. 1. In addition, the distributor is cylindrical (non-conical) and the guide vanes are not twisted along the radius. It was originally designed and tested by Souza (1989), who used free vortex hypothesis and blade element theory (this is a classical design procedure). This design will be referred to as the initial design and will be useful for comparisons with the optimization results. Table 1 shows some design basic features of this turbine.
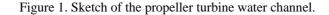
The flow through the turbine is considered incompressible and axisymmetric. The solver is a MatLab™ code based on the conservation principles for mass and angular momentum. The flow losses and deviations are assessed by using empirical correlations from open literature (Horlock, 1973).

In a previous work (Albuquerque *et al.*, 2005), the meridional velocity distributions were assumed to be uniform along the span. This is physically satisfactory only if the hypothesis of uniform blade specific work is also attained. However, in the mentioned work, a blade specific work variation of about 1:5 occurred from root to tip stations, contradicting the initial hypothesis. Therefore, the correct radial equilibrium must be evaluated in order to achieve a more realistic flow field. In the present work, the velocity distributions behind the stator and behind the runner are calculated according to the well known radial equilibrium condition. This is a relation between meridional and

circumferential absolute velocity components in conformity to energy conservation and momentuum equation in the radial direction – radial equilibrium equation (Manzanares-Filho, 1994).

A geometrical parameterization for reducing the number of design variables is also proposed in the present work.

Figure 1. Sketch of the propeller turbine water channel.

Table 1 - Turbine main features (Souza, 1989).

Flow rate	0.286 m³/s
Rotational speed	1145 rpm
Head	4.0 m
Design efficiency	85 %
Power output	9.5 kW
External diameter	280 mm
Internal diameter	112 mm
Number of blades	4
Guide vanes exit angle	60° (from tangential)

3.2. Blade geometry parameterization

The blade profile camber lines are approximated by arcs of circumference of small curvature, which is reasonable for an axial hydraulic turbine runner (whose blade profiles are typically little cambered). The blade thicknesses are not considered in this work, since no cavitation phenomena or flow separation is evaluated by the adopted modeling. Actually, when the blade profiles are thin enough, the thickness does not contribute to the hydrofoil lift: in a thin, small cambered hydrofoil, the thickness affects only the pressure distribution, the lift being a function only of the angle of attack and profile camber (thin airfoil theory – Karamcheti, 1980). As our main concern is the flow deflections in the guide vane and runner blade cascades, considering the camber lines only is enough to the evaluation of the flow field.

Thus the whole blade profile is defined by its stagger angle, β, chord-pitch ratio, ℓ/t, and relative camber at mid-chord, f/ℓ, Fig. 2. This choice for the runner design geometries is suitable since these three quantities lead to the cascade necessary geometric and kinematics characteristics in an initial design stage (as incidence angle, camber angle, angle of attack, deviation angle, flow deflection, etc.).
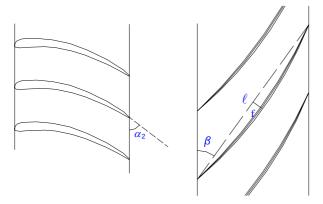

Figure 2. The design geometries in a radial station (cascade).

The runner blading stagger, chord-pitch ratio and camber spanwise variations are parameterized in terms of their values at the hub, mean and tip stations. A parameterization reduces the number of design variables and is used even for grid generation and grid modification (Lipej, 2004). In the present case, we have only 3×3 = 9 design variables for the

runner geometry. Among the various possibilities of parameterization, we have chosen parabolic functions. This choice is reasonable to approximate the usual geometric configuration found in axial hydraulic turbine designs (Lipej, 2004). In addition, the initial design of Souza (1989) – that was also parameterized for the comparisons with the optimized solution – is reasonably reproduced by the parabolic parameterizations, Fig. 3.

Because the guide vanes are not twisted along the radius, a single outlet angle, α_2, is enough as design variable for the distributor geometry (Fig. 2). So, we have a total of 9 + 1 = 10 design variables.

It must be emphasized that we are looking for a *conceptual* design optimization, in which the attained flow velocity distribution patterns are more relevant than the geometry itself. A complementary procedure could be an inverse cascade design optimization that would satisfy the inlet and outlet velocity profiles initially calculated. Actually, such approach has already been performed in more complex water turbine optimization problems (Lipej, 2004; Peng *et al.*, 2002). In these works, cavitation performance is also a problem objective – thus they are multiobjective optimization problems. As we have said before, the high computational cost in these schemes, however, is still a limitation factor to the design optimization course (Drtina and Sallaberger, 1999). Again, in the present work, we are looking for an intermediate methodology with low computational cost, being feasible to be performed in a single computer.
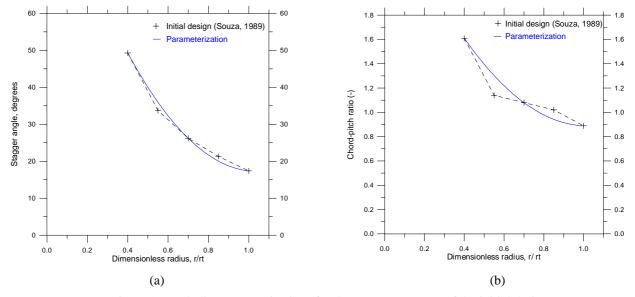

Figure 3. Parabolic parameterizations for the runner geometry of the initial design.

3.3. The radial equilibrium condition

Next we describe how the velocity distributions behind the distributor (stator) and behind the runner are evaluated in conformity to the radial equilibrium equation. The developments are referred to Figs. 4, 5, 6 and 7. The indexes *h* and *t* correspond respectively to hub and tip radial stations. *c* is the absolute velocity, *w* is the relative velocity and *u* is the blade velocity. α and β_f are respectively the absolute and relative flow angles, measured from circumferencial direction as shown in Fig. 5 and 6. The indexes *u* and *m* correspond respectively to circumferential and meridional velocity components. For example, c_{m5h} is the meridional component of the absolute velocity at runner exit and hub station.

3.3.1. Radial equilibrium behind the distributor

Assuming steady state, incompressible absolute flow in the stator, the energy equation (fist law of thermodynamics) leads to:

$$p_{S1} - p_{S2} = \rho Y_{Ls} \tag{1}$$

where p_S is the stagnation pressure, ρ is the specific mass and Y_{Ls} is the mechanical energy loss per unit mass in the stator.

The static pressure and absolute velocity are assumed to be constant at the distributor inlet, hence p_{S1} is constant along the span. Therefore, from the differentiation of Eq. (1), we have:

$$-\frac{dp_{S2}}{dr} = \rho \frac{dY_{Ls}}{dr} \tag{2}$$

The momentuum equation in the *r*-direction – radial equilibrium equation – is stated as follows:

$$\frac{dp_2}{dr} = \rho \frac{c_{u2}^2}{r} \tag{3}$$

where p is the static pressure. From Eqs. 2 and 3, the following relation between c_{m2} and c_{u2} can be derived (Manzanares-Filho, 1994):

$$c_{u2}\frac{d(rc_{u2})}{dr} + rc_{m2}\frac{dc_{m2}}{dr} + r\frac{dY_{Ls}}{dr} = 0 \tag{4}$$

This is the radial equilibrium condition behind the stator. If the spanwise distributions of c_{m2} and c_{u2} satisfy Eq. (4), these distributions are in agreement with the energy and momentuum equations. Although some simplifications have been made to derive Eq. (4), this relation leads to realistic trends for the flow field core in axial-flow turbomachines.

Observe that if we assume the free vortex condition (rc_{u2} = constant) and neglect the effect of the loss in the radial equilibrium ($dY_{Ls} / dr = 0$), we have c_{m2} = constant. Inversely, it can also be demonstrated that c_{m2} = const. $\Rightarrow rc_{u2}$ = const. The free vortex is a common design alternative and was used by Souza (1989) in the initial design. However, if the guide vane geometry does not furnish the free vortex at the enclosure between the stator and runner, c_{m2} will not be uniform along the span; thus, the correct radial equilibrium must be evaluated in order to achieve a realistic velocity distribution. Moreover, the free vortex condition is not necessarily the optimum one.
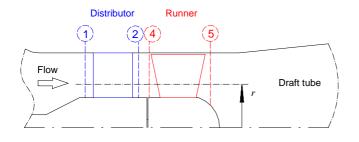

Figure 4. Meridional cross-section of turbine water channel.
1: distributor inlet;   2: distributor outlet
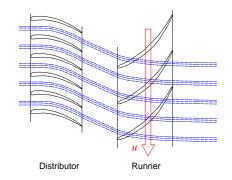4: runner inlet;   5: runner outlet

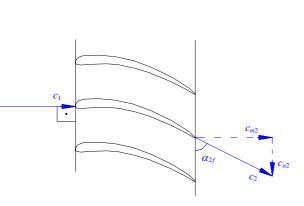Figure 5. Instantaneous absolute streamlines in a cylindrical section.

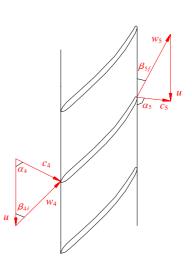Figure 6. Velocity components at distributor cascade.

Figure 7. Velocity triangles at runner cascade.

Neglecting the effect of the mechanical loss on the radial equilibrium (Peng *et al*., 2002) , Eq. 4 can be rewritten as:

$$\frac{d(c_{m2}^2)}{dr} = -\frac{1}{r^2}\frac{d(rc_{u2})^2}{dr} \tag{5}$$

The integration of Eq. (5) leads to the distribution of c_{m2} in terms of the velocity torque (rc_{u2}) variation, satisfying to the radial equilibrium along the whole span:

$$c_{m2}^2(r) - c_{m2h}^2 = \int_{r_h}^{r} -\frac{1}{r^2}\frac{d(rc_{u2})^2}{dr}dr = I_s(r) \tag{6}$$

$$c_{m2}(r) = \sqrt{c_{m2h}^2 + I_s(r)} \tag{7}$$

The overall continuity is now imposed in order to evaluate the meridional velocity at the hub station (c_{m2h}); Q is the volumetric flow rate:

$$Q = \int_{r_h}^{r_t} 2\pi c_{m2}(r)rdr \tag{8}$$

$$\int_{r_h}^{r_t} c_{m2}(r)rdr = Q/2\pi \tag{9}$$

$$\int_{r_h}^{r_t} \sqrt{c_{m2h}^2 + I_s(r)} \cdot rdr = Q/2\pi \tag{10}$$

Equation 10 is a nonlinear equation – with the unknown into an integration – to settle c_{m2h} according to the overall continuity and radial equilibrium condition. We have chosen a standard bisection algorithm from MatLab™ (fzero function) to solve this equation. The integration in Eq. (10) is evaluated by using the Simpson rule.

The evaluation of $I_s(r)$, Eq. (6), needs the previous knowledge of the velocity torque distribution, $rc_{u2}(r)$. However, the circumferential components c_{u2} are calculated by using the *not yet* determined meridional components c_{m2}. Therefore an iterative scheme must be adopted. We first assume a uniform distribution to c_{m2}. With this, some rc_{u2} values can be calculated by using cascade relations in *N* radial stations (cascades). These values are adjusted to a parabolic distribution by using least-squares. The choice of a parabolic distribution, $rc_{u2} = K_1 + K_2r + K_3r^2$, is indeed suitable for axial hydraulic turbines. This reproduces very well the typical swirl patterns (Peng *et al.*, 2002), can recuperate the free vortex (an important particular case) and has given great accuracy in our problem. Thence the adjusted parabolic distribution is used in the evaluation of $I_s(r)$ (which is performed analytically) and then the meridional velocity distribution (Eq. 7) can be evaluated after solving Eq. 10 for c_{m2h}. This new c_{m2} distribution is used now to recalculate the rc_{u2} values in cascades and the iterations are carried out until the flow field converges, Fig. 8.
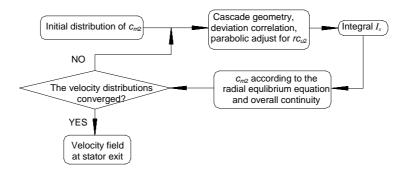

Figure 8. Iterative scheme for the velocity distribution evaluation behind the stator.

3.3.2. Radial equilibrium behind the runner

The velocity field at runner inlet is assumed to be equal the velocity field at stator exit, that has just been evaluated. Now, the energy equation gives:

$$p_{S4} = p_{S5} + \rho Y_{Lr} + \rho Y_{blade} \tag{11}$$

where Y_{Lr} is the mechanical energy loss per unit mass at runner and Y_{blade} is the blade specific work, calculated according to the Euler work equation:

$$Y_{blade} = u(c_{u4} - c_{u5}) \tag{12}$$

As we have neglected the effect of the hydraulic loss on the radial equilibrium behind the stator, the stagnation pressure at runner inlet is constant (see Eq. (2)):

$$\frac{dp_{S4}}{dr} = \frac{dp_{S2}}{dr} = -\rho \frac{dY_{Ls}}{dr} = 0 \tag{13}$$

The radial equilibrium equation is again stated as follows:

$$\frac{dp_5}{dr} = \rho \frac{c_{u5}^2}{r} \tag{14}$$

From Eqs. 11, 12, 13 and 14, and neglecting again the effect of the mechanical loss on the radial equilibrium (Peng *et al.*, 2002), an analogous development as that one for the stator leads to the following relation between c_{m5} and c_{u5}:

$$\frac{d(c_{m5}^2)}{dr} = -\frac{2(c_{u5}-u)}{r}\frac{d(rc_{u5})}{dr} - 2\frac{d(uc_{u4})}{dr} \tag{15}$$

This is the radial equilibrium condition behind the runner. Observe that the distribution of uc_{u4} is the same as that of uc_{u2}, which has just been determined in the previous subsection. Again, the integration of Eq. (15) leads to the distribution of c_{m5} satisfying to the radial equilibrium along the whole span:

$$c_{m5}^2(r) - c_{m5h}^2 = -2\int_{r_h}^{r}\frac{(c_{u5}-u)}{r}\frac{d(rc_{u5})}{dr}dr - 2\left(uc_{u4}\big|_r - uc_{u4}\big|_{r_h}\right) = I_r(r) \tag{16}$$

Again, the overall continuity is imposed in order to evaluate the meridional velocity at the hub station (c_{m5h}), leading to a nonlinear problem analogous to that for the distributor:

$$\int_{r_h}^{r_t}\sqrt{c_{m5h}^2 + I_r(r)}\cdot rdr = Q/2\pi \tag{17}$$

Due to the same considerations made on previous subsection, an analogous iterative scheme is newly adopted for the evaluation of the velocity distribution behind the runner, Fig. 9. Now, the N values of rc_{u5} in cascades are adjusted, by using least-squares, to a *cubic* function ($rc_{u5} = K_4 + K_5r + K_6r^2 + K_7r^3$) instead of a parabolic function. The choice of a cubic distribution has proved to be suitable for reproducing, with great accuracy, the typical inflections in c_{u5} spanwise variation. For the runner, however, a sub relaxation scheme had to be applied for attaining convergence. Each time a new distribution of c_{m5} is calculated (Eqs. 17 and 16), leading to a new c_{u5} distribution in cascades (from velocity triangles and deviation correlation), the new values settled to c_{u5} are given by:

$$c_{u5}^{new} = \lambda c_{u5}^{cascade} + (1-\lambda)c_{u5}^{old} \tag{18}$$

where λ is the sub relaxation factor. For starting this scheme, the first c_{u5} distribution is equated to zero. The sub relaxation factor has been settled equal to 0.10.
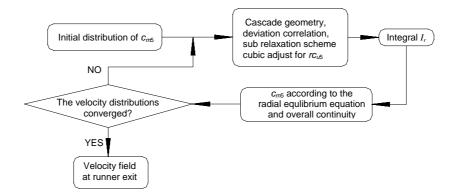

Figure 9. Iterative scheme for the velocity distribution evaluation behind the runner.

3.4. Loss and deviation correlations; turbine efficiency

The empirical loss correlations used in this study in order to calculate the losses through an axial hydraulic turbine are summarized in Tab. (2). Further details are found in Albuquerque *et al*. (2005).

The flow deviation with regard to the cascade metal angle is assessed by using the correlation of Carter and Hughes (Horlock, 1973). For example, the deviation angle at stator exit, δ, is given as:

$$\delta = \alpha_{2f} - \alpha_{2vane} = m\phi\sqrt{t/\ell} \tag{19}$$

where α_{2f} is the flow angle, α_{2vane} is the guide vane geometrical angle, ϕ is the profile camber angle ($\phi = \alpha_{1vane} - \alpha_{2vane}$), ℓ is the profile chord, t is the spacing and m is an empirical factor. In Horlock (1973), m is graphically provided as a function of the stagger angle, α (in degrees), and the kind of camber line (circular or parabolic). This graph was approximated by the linear function $m(\alpha) = 0.21 - 0.04(90 - \alpha)/60$, for circular camber lines adopted in this work. The flow deviation at the runner exit is evaluated analogously to that at stator exit, with the corresponding runner blade geometry (Albuquerque *et al*., 2005).

The losses are evaluated in N radial stations (cascades) and these values are adjusted to a cubic function by using least-squares. Thence, these regressions are integrated along the span in order to evaluate the total hydraulic loss, P_L. The runner blade specific work (Eq. (12)) is integrated along the span in order to calculate the total blade power, P_{blade}. From these results, we calculate the available head, $H = (P_{blade} + P_L)/(\rho gQ)$, the hydraulic efficiency, $\eta_h = P_{blade}/(P_{blade} + P_L)$ and the overall efficiency, $\eta = \eta_h\eta_{mec}$. All these calculations are performed by a MatLab™ code, this being the solver, whose flowchart is synthesized in Fig. 10.

Table 2 - The set of loss models used for axial hydraulic turbines.

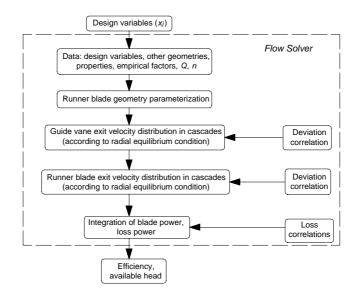| Loss mechanism	Loss model	Reference
Guide vane profile loss (skin friction loss at stator)	$$Y_{Ls} = \xi_s c_2^2 / 2$$	Horlock (1973)
Incidence loss (shock loss at runner inlet)	$$Y_{Linc} = \lambda w_{inc}^2 / 2$$ where $\lambda = 0.5$ to 0.7 and $$w_{inc} = \left(\frac{c_{m4}}{\tan\beta_{4blade}} + \frac{c_{m4}}{\tan\alpha_{2f}} \right) - u$$	Pfleiderer and Petermann (1979)
Runner blade profile loss (skin friction loss at runner)	$$Y_{Lr} = \xi_r w_5^2 / 2$$	Horlock (1973)
Draft tube loss (diffusion and swirl losses)	$$Y_{Ldt} = X_{Dm} \frac{c_{m5}^2}{2} + X_{Du} \frac{c_{u5}^2}{2}$$ where $X_{Dm} = 0.09$ to 0.12 and $X_{Du} = 0.20$ to 0.40	Raabe (1985)
Mechanical loss (external loss)	$\eta_{mec} = 0.96$ to 0.99	Adopted
	Coefficients for the profile loss (correlation of Soderberg): $$\xi = (10^5 / R_e)^{1/4}[(1+\xi_1)(0.975 + 0.075b/B) - 1]$$ $$\xi_1 = \xi_0 e^{0.01053\varepsilon} , \quad \xi_0 = 0.04 \text{ to } 0.06$$ $\varepsilon = \alpha_{1f} - \alpha_{2f}$ or $\varepsilon = \beta_{4f} - \beta_{5f}$ (flow deflection) B/b = radial/axial blade lengths (cascade aspect ratio) $R_e = \rho V D_h/\mu$, $V = c_2$ or w_5 , μ = dynamic viscosity $D_h = 2Bt\cos\alpha_{2f} /(t\cos\alpha_{2f} + B)$ or $D_h = 2Bt\cos\beta_{5f} /(t\cos\beta_{5f} + B)$	Horlock (1973)

Figure 10. Overall scheme of the solver code.

4. The optimization algorithms

Two optimization techniques have been used: a gradient based local search algorithm and a population set-based direct search algorithm.

The fmincon function from MatLab™ optimization toolbox was chosen as the local search algorithm. It consists in a standard constrained sequential quadratic programming (SQP) with line-search. The directional derivatives are evaluated by finite differences and the Hessian matrix is approximated by using the BFGS formula. In section 2 we have already described the framing of the standard constrained minimization problem and fmincon performs such scheme. The two main drawbacks of this optimization method are the search for local minimizers only and the need of a starting point. These two features together make the success of the search very depended on the initial guess for the design variables. Therefore the designer must beforehand know a configuration not far from the optimum. Also, the attained solution, presuming the convergence of the method, may not be the global optimum. Moreover, previous investigations have shown that even slightly different starting points can produce distinct solutions with different values of efficiency.

To overcome these limitations, it has also been proposed the application of a global search method, namely a Controlled Random Search Algorithm (CRSA). Like genetic and differential evolution algorithms, CRSA is a population set-based algorithm, which starts from an initial population of points on the problem feasible region and then performs iterative substitutions of worst points by better trial points in order to make the population converging to a global optimizer. In CRSA, a single point is replaced per iteration. The CRSA was chosen due to its simpler implementation, fastness and good results reported in technical literature (Albuquerque *et al.*, 2006).

The main convenience of this optimization technique is that it does not need a starting guess. Instead of an initial point – that the designer should evaluate with some care – the method employs an initial population randomly chosen on the feasible region. Setting up bounds for the design variables is easier than to set up a good initial design. Furthermore, there is the hope of finding a global solution, even with different feasible regions. A relatively small number of function evaluations is also an important feature of CRSA. This is particularly important when the objective function demands a high computational effort – what often occurs in turbomachine optimization.

When using CRSA, the available head constraints are imposed by means of a penalty scheme on objective function, as we have already described in section 2.

5. Optimization results

Previous investigations about the initial design of Souza (1989) were carried out with the developed solver. These studies have shown that, for fair comparisons, the optimization runs should be performed according to Table 3 for design point and head constraints and Table 4 for design variables lower and upper bounds.

Table 3. Design point and head constraints.

Flow rate, Q	0.288 m³/s
Rotational speed, n	1145 rpm
Lower head, H_L	3.5 m
Upper head, H_U	3.7 m

Table 4. Design variables lateral constraints.

Design Variable	β (°)			ℓ/t ($-$)			f/ℓ (%)			α_2 (°)
	hub	mean	tip	hub	mean	tip	hub	mean	tip	
x_j^L	40	25	15	1.61	1.08	0.889	0.8	0.5	0.1	50
x_j^U	55	35	25	1.70	1.20	1.00	6.0	4.0	2.0	70

Running on a Pentium4™ 3.0 GH$_Z$, the `fmincon` optimization courses take about two minutes only. For the CRSA optimizations, it is spent about fifteen minutes, which is also a reasonable time. Due to the stochastic features of CRSA, any CRSA solution should be taken in statistic sense. Actually, one should run several times the design optimization code to accept a solution. If the solver demands high computational effort and the global optimization method evaluates function values too many times, it would be prohibitive to perform a statistic study, or even to perform a single optimization run until achieving the stopping criterion.

Table 5 shows three solutions and their respective performance prediction found by using `fmincon` starting from different initial points $\mathbf{x}_0$. The values marked with an asterisk correspond to an activated constraint. The first solution was found starting from the initial design of Souza (1989). It should be noted the distinct optima values for the guide vanes outlet angle, α_2. This is a main concern since the distributor exit flow strongly affects the remaining runner blade geometry.

Table 5. Comparison of three `fmincon` solutions.

Design Variables and Resulting Quantities	`fmincon 1` $\mathbf{x}_0$ = (49.3 26.2 17.4 1.61 1.08 0.889 0 0 0 60)			`fmincon 2` $\mathbf{x}_0$ = (55.0 32.0 25.0 1.61 1.08 0.889 0.8 0.5 0.2% 51)			`fmincon 3` $\mathbf{x}_0$ = (40.0 25.0 15.0 1.61 1.08 0.889 0.8 0.5 0.2% 68)		
	hub	mean	tip	hub	mean	tip	hub	mean	tip
β (°)	49.4	28.7	18.7	55.0*	30.1	23.3	40.5	27.4	17.5
ℓ/t ($-$)	1.61*	1.08*	0.889*	1.614	1.08*	0.889*	1.61*	1.08*	0.889*
f/ℓ (%)	3.64	1.67	0.93	5.87	2.17	0.1*	3.34	1.22	1.19
α_2 (°)	60.7			50.5			68.9		
Blade power (W)	9218			9046			9208		
Distributor loss (W)	211			278			178		
Runner + draft tube loss (W)	1011			1040			1104		
η (%)	84.77			83.79			84.27		
H (m)	3.70 *			3.70 *			3.70 *		

Actually, the first solution shown above is the best design that has been achieved by using `fmincon` starting from various different initial points. Thus it seems that `fmincon` 1 is perhaps the global optimum.

The analysis of the second solution shows that its guide vanes outlet angle (= 50.5°) is very small. This distributor gives too much angular momentum to the flow at runner inlet. Due to the available head upper bound (= 3.7 m), the runner can not extract all this angular momentum in order to produce an exit flow without swirl. Therefore, we have a positive swirling flow at runner exit, which leads to less blade power and a little more runner and draft tube losses than those of the first solution. In addition, the excessive guide vane deflection increases considerably the distributor loss (32%). As a final result, the efficiency of the `fmincon` 2 solution is 1% lower than that of `fmincon` 1.

On the other hand, the third solution has a great guide vanes outlet angle (= 68.9°). In this case, the flow at runner inlet presents a little angular momentum. Then, in order to produce a reasonable shaft power, the runner blades deflect the flow in a way that the exit swirling is highly negative. This deflection leads to an increase of 10% in the runner and draft tube losses. Although the distributor loss is now lower than that of `fmincon` 1 solution, the efficiency is 0.5% inferior.

The `fmincon` 1 solution for the distributor, $\alpha_2 = 60.7°$, probably leads to the optimum angular momentum at runner inlet. This makes possible the most efficient absorption of the flow energy by the runner blades. Actually, the flow at runner inlet must occur with minimum shock (which is also important to avoid cavitation risk) and the blading stagger and camber must be such that reasonable flow deflections and a minimum swirling exit flow take place. The adopted loss and deviation modeling with the geometry parameterization and the imposition of the radial equilibrium condition indeed allow the optimizer to searching for these correct trends in hydraulic turbine design. In addition, the original design of Souza (1989) is already a good solution, mainly due to the very good choice for α_2 (= 60.0°, Tab. (1)). However, this turbine is still open to improvements in the runner geometry.

Table (6) compares directly the initial design with the optimized one, showing the performance improvements. It is also shown the solution found by using the CRSA (Albuquerque *et al.*, 2006). It must be noted the good agreement between the best `fmincon` solution (i.e., `fmincon` 1) and the CRSA solution. Therefore, the global optimum has probably been achieved and we will refer to `fmincon` 1 as the optimized design.

Table 6. Comparison of initial design, best `fmincon` solution and CRSA solution.

Design Variables and Resulting Quantities	**Initial design** (Souza, 1989)			**fmincon 1** (present work)			**CRSA solution** (Albuquerque *et al.*, 2006)		
	hub	*mean*	*tip*	*hub*	*mean*	*tip*	*hub*	*mean*	*tip*
β (°)	49.3	26.2	17.4	49.4	28.7	18.7	49.5	29.0	18.6
ℓ/t ($-$)	1.61	1.08	0.889	1.61	1.08	0.889	1.65	1.09	0.890
f/ℓ (%)	straight blade assumed			3.64	1.67	0.93	3.69	1.77	1.02
α_2 (°)	60.0			60.7			60.5		
Blade power (W)	8761			9218			9178		
Distributor loss (W)	215			211			213		
Runner + draft tube loss (W)	1443			1011			1011		
η (%)	80.72			84.77			84.71		
H (m)	3.70			3.70			3.70		

Note again that the guide vanes outlet angle is essentially the same in both designs, that is, the initial design of Souza (1989) for the distributor is already well optimized. The runner, however, can be improved. Figure 11 compares the spanwise variations of some runner blade geometry in the initial and optimized designs. The main difference is that the stagger angle can be a little increased along the whole span (the blades being more opened). The camber is also adjusted by the optimizer so that a small incidence loss at runner inlet (Fig. 15) and a little swirling flow at runner outlet (Figs. 13 and 14) take place. The optimized runner blading stagger and camber are represented in Fig. 12.

In Figs. 13 and 14 we see the velocity distributions for both designs. Due to the very small difference between both guide vanes outlet angles, the distributions of c_{m2} and c_{u2} are very close between the initial and optimized designs. At runner exit, however, the swirl and meridional velocity components are different. In the initial design, we have a great spanwise variation in c_{m5}; the optimized geometry produces a more uniform exit flow, decreasing the meridional component of the draft tube loss (Tab. (2)). While the flow exit swirl is everywhere positive in the initial design, the optimized solution produces a negative swirl near the hub and a positive one at the tip. This trend is in good agreement with flow measurements in well designed axial hydraulic turbines (Vivier, 1966).

Figure 15 shows the spanwise variation of the specific losses. The main improvements are in the incidence and draft tube losses, as we have already explained. As the losses are integrated on a mass flux basis, it is also plotted the sum of runner and draft tube losses (∆), showing the significant decrease achieved by the optimization (=30%, Tab. (6)).

In Fig. 16 we have the spanwise distribution of the blade specific work. In comparison with the initial design, the optimized solution increased the specific work along the whole span. In addition, the flow deflections by the runner, not shown in this work, are yet within feasible values for axial-flow hydraulic turbine blade profiles, varying from 17° at the hub to 3° at the tip. This is also important for avoiding cavitation risk, since the blade loading has a direct impact in cavitation phenomena.
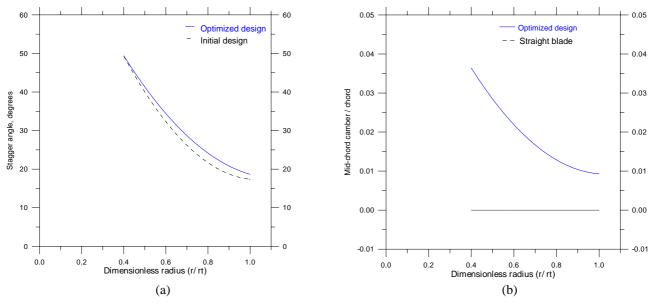
(a) (b)

Figure 11. Runner blading (a) stagger and (b) camber of initial design and optimized solution.
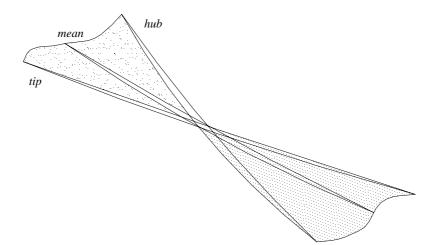

Figure 12. Optimized runner blade (the thicknesses are only illustrative).
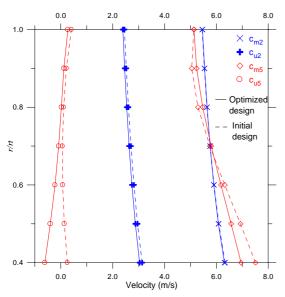

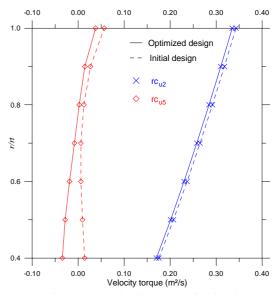Figure 13. Flow velocity distributions.

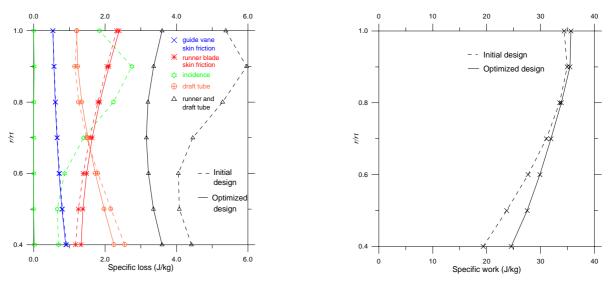Figure 14. Velocity torque distributions.

Figure 15. Spanwise loss variations.

Figure 16. Spanwise blade specific work distribution.

6. Conclusion

The conceptual design optimization of axial-flow hydraulic turbines can be performed by using the present methodology. The adopted loss and deviation modeling with the geometrical parameterization and the imposition of the radial equilibrium condition indeed allow the optimizer to search for the correct geometrical and flow trends in axial hydraulic turbine design.

Cavitation phenomena are not considered in the present work, since the main concern is the flow deflections in the guide vane and runner blade cascades. The simplified geometry for the runner blades, considering the profile camber lines only, is enough to the evaluation of the velocity field in this intermediate design approach.

A complementary design procedure could be an inverse cascade design optimization that would satisfy the inlet and outlet velocity profiles initially calculated.

7. References

Albuquerque, R. B. F., Manzanares-Filho, N. and Oliveira, W., 2005, "Optimized design of axial-flow hydraulic turbine", Proceedings of 18th International Congress of Mechanical Engineering, paper No. 1695.

Albuquerque, R. B. F., Manzanares-Filho, N. and Oliveira, W., 2006, "A study of controlled random search algorithms with application to conceptual design optimization of axial-flow hydraulic turbines", to appear in Proceedings of XXVII Iberian Latin-American Congress on Computational Methods in Engineering.

Cordier, O., 1955, "Ähnlichkeitsbetrachtung bei Strömungsmaschinen", VDI-Zeitschrift, Vol. 97, No. 34, pp. 1233-1234.

Drtina, P. and Sallaberger, M., 1999, "Hydraulic turbines – basic principles and state-of-the-art computational fluid dynamics applications", Proc. Instn. Mech. Engrs., Vol. 213, part C, pp. 85-102.

Horlock, J. H., 1973, "Axial Flow Turbines", Robert E. Krieger Plublishing Company, Huntington, USA, 275 p.

Karamcheti, K., 1980, "Principles of Ideal-Fluid Aerodynamics", Robert E. Krieger Plublishing Company, Florida, USA, 636 p.

Lipej, A., 2004, "Optimization method for the design of axial hydraulic turbines", Proc. Instn. Mech. Engrs., Vol. 218, part A, pp. 43-50.

Manzanares-Filho, N., 1994, "Flow Analysis of Axial Flow Turbomachines" (in Portuguese), Doctoral Thesis, Technological Institute of Aeronautics, São José dos Campos, Brazil.

Oh, H. W. and Kim, K.-Y., 2001, "Conceptual design optimization of mixed-flow pump impellers using mean streamline analysis", Proc. Instn. Mech. Engrs., Vol. 215, part A, pp. 133-138.

Vivier, L., 1966, "Turbines Hydrauliques et leur régulation", Éditions Albin Michel, Paris, France, 581 p.

Peng, G., Cao, S., Ishizuka, M. and Hayama, S., 2002, "Design optimization of axial flow hydraulic turbine runner: Part I – an improved Q3D inverse method", IJNMF, Vol. 39, pp. 517-531.

Pfleiderer, C. and Petermann, H., 1979, "Máquinas de Fluxo", LTC, Rio de Janeiro, Brazil, 454 p.

Raabe, J., 1985, "Hydro Power", VDI Verlagembh, Dusseldof, Germany, 683 p.

Schweiger, F. and Gregori, J., 1989, "Design of Large Hydraulic Turbines", IAHR Symposium, Beijing, pp. 155-164.

Souza, Z., 1989, "Test and Operation Reports for The MEP Tube Type Hydraulic Turbine", Private report, in Portuguese, UNIFEI, Itajubá, Brazil.

Yoon, E. S., Kim, B. N. and Chung, M. K., 1998, "Modeling of three dimensional unsteady flow effects in axial flow turbine rotors", Mechanics Research Communications, Vol. 25, No. 1, pp. 15-24.

6. Copyright Notice